Evaluation of ^{131}I-Anti-Angiotensin II Type 1 Receptor Monoclonal Antibody as a Reporter for Hepatocellular Carcinoma

Pan-Pan Hao[1,2]☌, Yan-Ping Liu[1]☌, Chang-Ya Yang[1], Ting Liang[1], Chao Zhang[1], Jing Song[1], Jian-Kui Han[3], Gui-Hua Hou[1]*

1 Key Laboratory for Experimental Teratology of the Ministry of Education and Institute of Experimental Nuclear Medicine, School of Medicine, Shandong University, Jinan, China, 2 The Key Laboratory of Cardiovascular Remodeling and Function Research, Chinese Ministry of Education and Chinese Ministry of Health, Qilu Hospital, Shandong University, Jinan, China, 3 Department of Nuclear Medicine, Qilu Hospital, Shandong University, Jinan, China

Abstract

Background: Finding a specific agent is useful for early detection of tumor. Angiotensin II type 1 receptor (AT$_1$R) was reported to be elevated in a variety of tumors and participate in tumor progression. The aim of our study was to evaluate whether ^{131}I-anti-AT$_1$R monoclonal antibody (mAb) is an efficient imaging reporter for the detection of hepatocellular carcinoma.

Methodology/Principal Findings: AT$_1$R mAb or isotype IgG was radioiodinated with ^{131}I and the radiochemical purity and stability of the two imaging agents and the affinity of ^{131}I-anti-AT$_1$R mAb against AT$_1$R were measured. 3.7 MBq ^{131}I-anti-AT$_1$R mAb or isotype ^{131}I-IgG was intravenously injected to mice with hepatocellular carcinoma through tail vein, and then the whole-body autoradiography and biodistribution of the two imaging agents and the pharmacokinetics of ^{131}I-anti-AT$_1$R mAb were studied. ^{131}I-anti-AT$_1$R mAb and ^{131}I-IgG were successfully radioiodinated and both maintained more stable in serum than in saline. The ^{131}I-anti-AT$_1$R mAb group showed much clearer whole-body images for observing hepatocellular carcinoma than the ^{131}I-IgG group. The biodistributions of the two imaging agents suggested that hepatocellular carcinoma tissue uptook more ^{131}I-anti-AT$_1$R mAb than other tissues (%ID/g = 1.82±0.40 and T/NT ratio = 7.67±0.64 at 48 h), whereas hepatocellular carcinoma tissue did not selectively uptake ^{131}I-IgG (%ID/g = 0.42±0.06 and T/NT ratio = 1.33±0.08 at 48 h). The pharmacokinetics of ^{131}I-anti-AT$_1$R mAb was in accordance with the two-compartment model, with a rapid distribution phase and a slow decline phase. These results were further verified by real-time RT-PCR, immunohistochemistry staining and Western blot.

Conclusions/Significance: ^{131}I-anti-AT$_1$R mAb may be a potential target for early detection of tumor.

Introduction

Hepatocellular carcinoma is the sixth most prevalent cancer and the third most frequent cause of cancer-related death [1,2]. Although biopsy is considered to be the gold standard for diagnosis of hepatocellular carcinoma, it is more invasive than serum biomarkers or imaging techniques. The detection of hepatocellular carcinoma mainly relies on serum alpha-fetoprotein and liver imaging techniques such as B-mode ultrasound, X-ray computed tomography, magnetic resonance imaging and positron emission computed tomography [3–5]. But when these abnormalities can be detected, the staging of hepatocelluar carcinoma usually goes into an advanced symptomatic stage [1]. Therefore, exploring a new non-invasive technology to detect hepatocellular carcinoma in a very early stage is urgently needed. Molecular imaging is such a technology, which integrates the principles of cell and molecular biology, immunology, nuclear medicine and diagnostic imaging [6]. Then it becomes an issue to find a target molecule which could specifically detect tumor in an early stage.

Overexpression of angiotensin II type 1 receptor (AT$_1$R) in a variety of tumors has been reported recently [7–10]. AT$_1$R promotes tumor growth and angiogenesis partially through upregulation of vascular endothelial growth factor (VEGF) [11,12]. We hypothesized that AT$_1$R expression might be upregulated in hepatocellular carcinoma tissue and ^{131}I-anti-AT$_1$R IgG monoclonal antibody (mAb) might be a new potential molecular imaging agent in tumor. The aim of this study was to validate this hypothesis.

Materials and Methods

Ethics statement

The animal protocol was reviewed and approved by the Institutional Animal Care and Use Committee at School of Medicine, Shandong University.

Cell culture and reagents

Murine hepatocellular carcinoma cell line H22 (Cell Bank of Chinese Academy of Sciences, Shanghai, China), murine liver cell line NCTC clone 1469 (CCL-9.1, American Type Culture Collection, Manassas, VA), human cervical cancer cell line Hela (CCL-2, American Type Culture Collection) and rat adrenal pheochromocytoma cell line PC12 (CRL-1721, American Type Culture Collection) were cultured in RPMI 1640 medium (Invitrogen, Carlsbad, CA), all supplemented with 100 units·mL^{-1} penicillin (Gibco BRL, Gaithersburg, MD), 100 units·mL^{-1} streptomycin (Gibco BRL) and 10% fetal bovine serum (Gibco BRL) at 37°C in a 95% air/5% CO$_2$ humidified atmosphere.

Animal model

Male BALB/c mice (6–8 weeks old) were purchased from Shandong University Animal Center and were maintained under pathogen-free conditions. The BALB/c mice (36 per group) were injected subcutaneously with 1×10^7 H22 cells in 0.1 mL phosphate buffered saline into the right upper back to establish a hepatoma model.

Radioiodination of anti-AT$_1$R mAb and isotype IgG

50 µg anti-AT$_1$R mAb (Abcam, Cambridge, UK) or isotype IgG (Abcam) was iodinated with 15 µL Na^{131}I (185 MBq) (China Institute of Atomic Energy, Beijing, China) using the Iodogen method as described previously [13]. Radioiodinated anti-AT$_1$R mAb and isotype IgG were separated from free iodine using size exclusion columns (Sephadex G-25, Amersham Pharmacia Biotech, Uppsala, Sweden).

Radiochemical purity and stability

Radiochemical purity was determined by paper chromatographic method using strips on two-paper sheet (1 cm width and 13 cm length) as described [14] with modifications. Briefly, an aliquot of 2 µL ^{131}I-anti-AT$_1$R mAb or ^{131}I-IgG was added into 400 µL serum or saline. 2 µL of the mixture was placed 2 cm above the lower edge and was allowed to evaporate spontaneously, one strip was developed with acetone and the other was developed with ethanol: water: ammonium hydroxide mixture (2:5:1). After complete development, the paper sheet was removed, dried, and cut into strips of 1 cm width; and then each strip was counted in a well-type c-counter. The percentage of radiochemical yield was calculated as the ratio of the radioactivity of ^{131}I-anti-AT$_1$R mAb or ^{131}I-IgG to the total activity multiplied by 100. Radiochemical purities were measured at 1, 6, 24, 48, 72 and 96 hours, respectively, to assess the stability.

Radioligand-based binding assay

The radioligand-based binding assay was carried out in borosilicate glass tubes as described [15,16] with modifications. For saturation studies, a reaction mixture contained 200 µL H22 cells (5×10^6/mL) and 100 µL ^{131}I-anti-AT$_1$R mAb (0.1–32 nM, diluted in $1 \times$PBS) in a final volume of 500 µL. 10^{-1}–10^5 nM unlabeled anti-AT$_1$R mAb and 12 nM ^{131}I-anti-AT$_1$R mAb were used for competition binding assay. The mixture was incubated at 37°C for 2 h. The bound radioligand was separated by rapid vacuum filtration through Whatman GF/B filters using a cell harvester followed by 3×2 mL washes of PBS at room temperature. The radioactivity of filters containing the bound radioligand was assayed in test tube by Wipe Test/Well Counter (Caprac; Capintec, Ramsey, NJ). The results of saturation and inhibition experiments were subjected to nonlinear regression analysis and the equilibrium dissociation constant (K$_D$), the maximum number of binding sites (B$_{max}$), the inhibitor constant (K$_i$) and the half maximal inhibitory concentration (IC$_{50}$) were calculated.

Whole-body autoradiography

Whole-body autoradiography was performed as described [17] with modifications. 10% potassium iodide was added to drinking water 3 days before injection of ^{131}I-labeled antibody to block the thyroid gland. 12 days after injection of H22 cells, 3.7 MBq ^{131}I-anti-AT$_1$R mAb or ^{131}I-IgG was respectively injected into the mice through tail vein. Whole-body autoradiography was performed at 1, 6, 24, 48 and 72 hours after injection, respectively. The anesthetized mice were fixed on the storage phosphor screen plate in supine position with four limbs stretched in order to make the tumor tightly close to the plate. The plate was exposed to a mouse for 15 minutes in a darkroom. After exposure, the plate was scanned by Cyclone Plus Storage Phosphor System (PerkinElmer) and analyzed using the OptiQuant Acquisition software.

Biodistribution of ^{131}I-anti-AT$_1$R mAb and ^{131}I-IgG

Six mice of each group were sacrificed at 1, 6, 24, 48 and 72 hours after injection, respectively, and blood, tumor, muscular tissue on the left side and main organs were removed, weighed, and counted radioactivity in the gamma counter. The percent injected dose per gram (%ID/g) and target to non-target ratio (T/NT) were calculated.

Pharmacokinetic analysis

10 µL blood samples were taken from periorbital vein of six mice at 0, 1, 3, 6, 12, 24, 48, 72, 96 and 120 hours after injection of ^{131}I-anti-AT$_1$R mAb and then the radioactivity was measured by Liquid Scintillation Counting. The distribution half-life (T$_{1/2\alpha}$), the elimination half-life (T$_{1/2\beta}$) and the mean residence time (MRT) were calculated.

Real-time PCR

The primer for AT$_1$R was chosen in cDNA portions by accessing mouse sequences in GenBank. The sequences were as follows: sense primer, 5′-GAAGAACAAGCCAAGAAATGATG-3′; antisense primer, 5′-TTGATGACTCCAGGTTAGCAGAT-3′ (887 bp). Total RNA was extracted from the cell lines or freshly isolated tumor, contralateral muscle and normal liver tissue by use of TriZol reagent (Invitrogen, Carlsbad, CA). Oligo (dT) primed cDNA synthesis involved use of Superscript^{TM}III reverse transcriptase (Invitrogen). Transcripts were amplified from reverse-transcribed cDNA by use of SYBR Green (Invitrogen). Cycling conditions for amplification were as follows: 4 min, denaturation step at 94°C; followed by 35 cycles of 30 s, at 94°C, 1 min, at 55°C, and 1 s, at 72°C. Quantitative assessment of relative gene expression levels involved the $2^{-\triangle\triangle CT}$ method.

Histology

Tissues were fixed in phosphate-buffered 4% paraformaldehyde, embedded in paraffin, and cut into 4-µm thick sections. Sections were deparaffinized and stained with hematoxylin and eosin using a standard protocol to determine morphology. AT$_1$R protein expression was determined by immunostaining with anti-

AT$_1$R mAb (1:50) using the streptavidin-biotin method. Image-Pro Plus v5.0.2 (Media Cybernetics, Inc., Bethesda, MD) was used for quantitative assessment of relative AT$_1$R protein expression levels.

Western blot

SDS polyacrylamide gel electrophoresis and Western blot analysis were performed as described previously [18]. Membranes were incubated with anti-AT$_1$R mAb (1:400) or a primary antibody against β-actin (1:1000; Cell Signaling Technology, Danvers, MA), followed by appropriate horseradish peroxidase-labeled secondary antibodies. Protein levels were normalized to that of β-actin as an internal control. HeLa cells and PC12 cells were used as positive controls.

Statistical analysis

SPSS v11.5 (SPSS Inc., Chicago, IL) was used for statistical analysis. Continuous data were expressed as mean ± SEM and compared by one-way ANOVA, followed by unpaired t-test or paired t-test as appropriate. A P value <0.05 was considered statistically significant.

Results and Discussion

Radioiodination of anti-AT$_1$R mAb and isotype IgG

^{131}I-anti-AT$_1$R mAb and ^{131}I-IgG were successfully radioiodinated. The radiochemical purity of ^{131}I-anti-AT$_1$R mAb was 92.8% and that of ^{131}I-IgG was 93.2%. The specific activity of ^{131}I-anti-AT$_1$R mAb was 35.24±5.76 MBq/μmol and that of ^{131}I-IgG was 38.61±7.18 MBq/μmol.
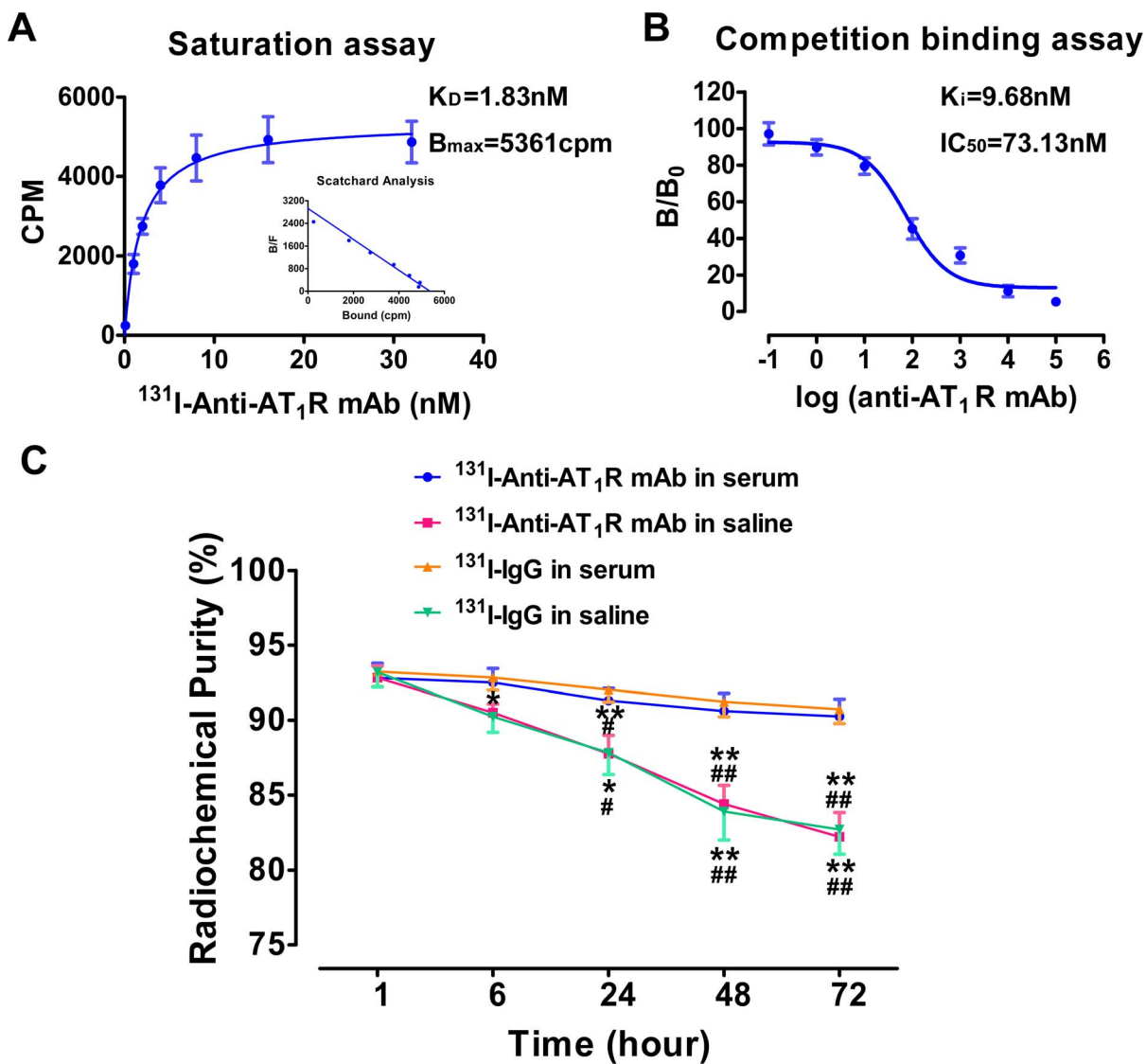
Figure 1. The affinity and stability of ^{131}I-AT$_1$R mAb and ^{131}I-IgG. (A) The saturation assay of ^{131}I-AT$_1$R mAb. K$_D$, equilibrium dissociation constant; B$_{max}$, maximum number of binding sites. (B) The competition binding assay of ^{131}I-AT$_1$R mAb. K$_i$, inhibitor constant; IC$_{50}$, half maximal inhibitory concentration. (C) The radiochemical purity of ^{131}I-AT$_1$R mAb and ^{131}I-IgG. *P<0.05 and **P<0.01 vs. 1 hour; #P<0.05 and ##P<0.01 vs. the same time-point in serum.
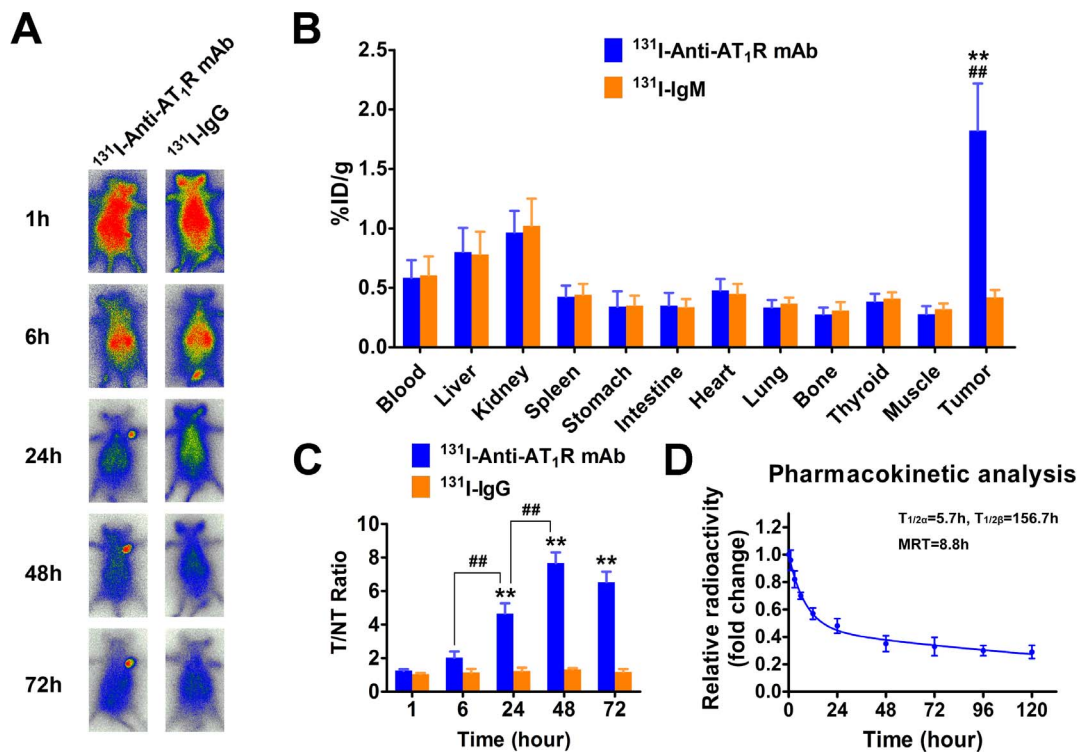
doi:10.1371/journal.pone.0085002.g001

Figure 2. The whole-body autoradiography and biodistribution of ^{131}I-anti-AT$_1$R mAb and ^{131}I-IgG in a mouse model of hepatocellular carcinoma. (A) The whole-body autoradiography. (B) The %ID/g of main tissues at 48 hours. **$P<0.01$ vs. muscle. ##$P<0.01$ vs. ^{131}I-IgG. (C) The T/NT ratios. **$P<0.01$ vs. 1 hour. ##$P<0.01$. (D) The pharmacokinetics analysis of ^{131}I-AT$_1$R mAb. T$_{1/2\alpha}$, distribution half-life; T$_{1/2\beta}$, elimination half-life; MRT, mean residence time.
doi:10.1371/journal.pone.0085002.g002

The affinity of ^{131}I-AT$_1$R mAb against AT$_1$R

Radioligand-based binding assay is one of the most sensitive techniques available to quantitatively determine the affinity of one antibody against a certain receptor. Saturation assay showed that ^{131}I-anti-AT$_1$R mAb displayed saturable binding with H22 cells and K$_D$ and B$_{max}$ were 1.83 ± 0.48 nM and 5361 ± 345.3 cpm, respectively. Transformation of the saturation binding of ^{131}I-anti-AT$_1$R mAb to Scatchard plots gave linear plots, suggesting that it involved a single population of binding sites (Fig. 1A). Competitive binding assay was also conducted with ^{131}I-anti-AT$_1$R mAb as radioligand. The unlabeled anti-AT$_1$R mAb competed effectively with ^{131}I-anti-AT$_1$R mAb binding sites on H22 cells at low micromole concentrations and K$_i$ and IC$_{50}$ were 9.68 ± 1.33 nM and 73.13 ± 1.33 nM, respectively (Fig. 1B). These results revealed high affinity of ^{131}I-anti-AT$_1$R mAb against AT$_1$R.

The stability of ^{131}I-AT$_1$R mAb and ^{131}I-IgG

The radiochemical purities of ^{131}I-anti-AT$_1$R mAb and ^{131}I-IgG were still over 90% in serum, and declined under 80% in saline at 72 hours, indicating that they maintained more stable in serum than in saline. There was no significant difference between the two imaging agents (Fig. 1C).

The whole-body autoradiography in the hepatoma mice

The ^{131}I-anti-AT$_1$R mAb group showed much clearer whole-body images for observing hepatocellular carcinoma than the ^{131}I-IgG group 24 hours after injection of radioiodinated anti-AT$_1$R mAb or isotype IgG and the difference reached a peak at 48 hours (Fig. 2A). These data demonstrate that the ^{131}I-anti-AT$_1$R mAb

appears to be more specific than ^{131}I-IgG for targeting hepatocellular carcinoma.

Biodistribution of ^{131}I-anti-AT$_1$R mAb and ^{131}I-IgG

In the ^{131}I-anti-AT$_1$R mAb group, %ID/g of the tumor was higher than that of other tissues, and T/NT reached a peak at 48 hours after injection (%ID/g $= 1.82\pm0.40$ and T/NT ratio $= 7.67\pm0.64$). In the ^{131}I-IgG group, there was no significant increase of %ID/g in the tumor and T/NT remained stable throughout the experiment (Fig. 2B and C). The results indicated that hepatocellular carcinoma tissue uptakes more ^{131}I-anti-AT$_1$R mAb than other tissues, whereas hepatocellular carcinoma tissue does not selectively uptake ^{131}I-IgG. Thus, ^{131}I-anti-AT$_1$R mAb may be a potential imaging agent for targeting hepatocellular carcinoma.

Pharmacokinetic analysis

Pharmacokinetic analysis showed that the pharmacokinetics of ^{131}I-anti-AT$_1$R mAb was in accordance with the two-compartment model, with a rapid distribution phase and a slow decline phase. T$_{1/2\alpha}$ and T$_{1/2\beta}$ were 5.7 h and 156.7 h, respectively, and MRT was 8.8 h (Fig. 2D).

AT$_1$R mRNA and protein expression

AT$_1$R mRNA expression was quantified by real-time RT-PCR. There was a markedly higher AT$_1$R mRNA level in H22 cells than that in NCTC clone 1469 cells (Fig. 3A). Similarly, there was a significantly higher AT$_1$R mRNA level in hepatocellular carcinoma tissue than that in contralateral muscle (control 1) or normal liver tissue (control 2) (Fig. 3C). AT$_1$R protein expression was
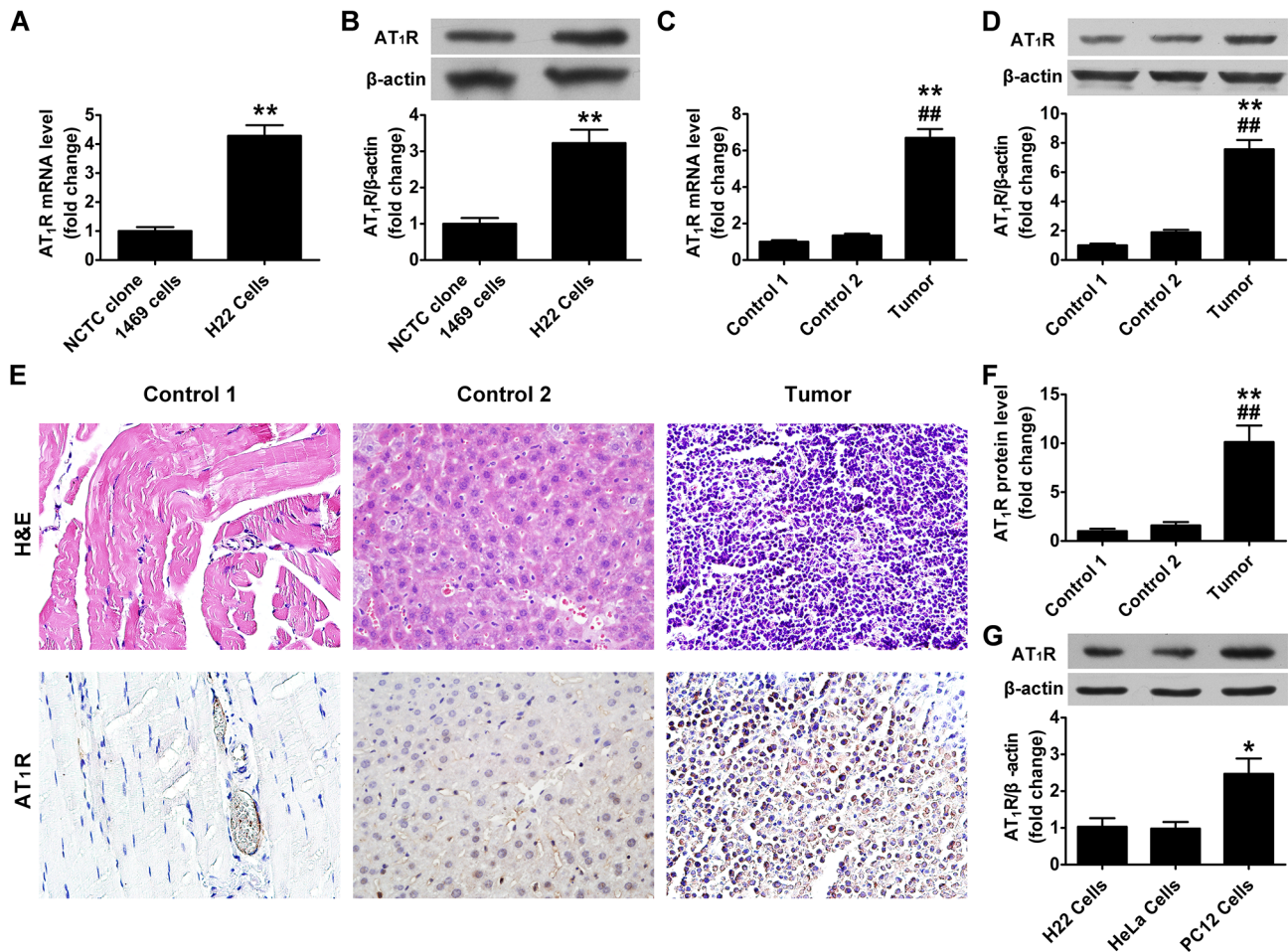
Figure 3. AT$_1$R mRNA and protein expression. (A) Relative mRNA expression of AT$_1$R in NCTC clone 1469 cells (normal hepatocytes) and H22 cells. **$P<0.01$ vs. NCTC clone 1469 cells. (B) Representative Western blot of AT$_1$R and quantification of AT$_1$R protein levels in NCTC clone 1469 cells and H22 cells. **$P<0.01$ vs. NCTC clone 1469 cells. (C) Relative mRNA expression of AT$_1$R in the muscle of the opposite side (control 1), normal liver tissue (control 2) and hepatocellular carcinoma tissue. **$P<0.01$ vs. control 1. $^{##}P<0.01$ vs. control 2. (D) Representative Western blot of AT$_1$R and quantification of AT$_1$R protein levels in control 1, control 2 and hepatocellular carcinoma tissue. **$P<0.01$ vs. control 1. $^{##}P<0.01$ vs. control 2. (E) Representative hematoxylin and eosin staining (H&E) and immunohistochemical staining for AT$_1$R (original magnification 400×). (F) Quantification of AT$_1$R protein levels in immunohistochemical staining. **$P<0.01$ vs. control 1. $^{##}P<0.01$ vs. control 2. (G) Representative Western blot of AT$_1$R and quantification of AT$_1$R protein levels in H22 cells, HeLa cells and PC12 cells. *$P<0.05$ vs. H22 cells.
doi:10.1371/journal.pone.0085002.g003

assessed by immunohistochemistry staining and Western blot. AT$_1$R protein was mainly localized to cell membranes (Fig. 3E). AT$_1$R protein level was significantly higher in H22 cells than that in NCTC clone 1469 cells (Fig. 3B). Similarly, AT$_1$R protein level was significantly higher in hepatocellular carcinoma tissue than that in control 1 or control 2 (Fig. 3D, 3F). In addition, AT$_1$R protein level was higher in PC12 cells than in H22 or HeLa cells (Fig. 3G).

Attempts have never ceased for diagnosis and surveillance of tumor. Although biopsy is still the gold standard for monitoring and predicting the process of tumor, early protocol biopsies can not be performed conventionally due to its invasive characteristic. Imaging examination becomes an ideal method owing to its noninvasive characteristic and good repeatability. Molecular imaging, which integrates imaging techniques with molecule biology, is more sensitive and can detect abnormalities before the appearance of symptoms and signs. Screening for optimal molecules as biomarkers plays a key role in molecular imaging. An ideal biomarker for tumor should be closely related to tumor progression, and absolutely or relatively specific for diagnosis and surveillance of tumor.

The utility of molecular imaging in hepatocellular carcinoma mainly relies on the non-invasive detection of cytokines or other molecules secreted by the tumor evenly before the functional and structural changes can be discovered [19,20]. The early detection of tumor could improve survival greatly and the benefits of molecular imaging should not be underestimated. Identification of novel targets and predictors through molecular cell biology will identify new diagnostic strategies for early stage hepatocellular carcinoma and provide better methods for outcome prediction.

The renin-angiotensin system (RAS) plays an important role in tumor growth and angiogenesis [21–23]. Ang II, the main effector peptide of RAS, was reported to be involved in the development of several tumors, including breast, ovarian and pancreatic cancers [24–26]. Ang II exerts a variety of biological actions through binding to AT$_1$R [27]. Thus, interference with AT$_1$R by declining the level of Ang II or antagonizing the receptor may impair tumor growth and angiogenesis [28].

This study suggested that AT$_1$R was overexpressed in hepatocellular carcinoma tissue using a mouse hepatoma model and revealed that hepatocellular carcinoma tissue could specifically uptake ^{131}I-anti-AT$_1$R mAb but not ^{131}I-IgG. In the early stage of imaging, the two agents were infiltrated in the intercellular space non-specifically through binding to the receptor of fragments crystallizable to IgG on the tissues. In the late stage of imaging, the non-specific accumulation of ^{131}I-IgG decreased gradually, while the specific accumulation of ^{131}I-anti-AT$_1$R mAb increased markedly, attributed to the increased expression of AT$_1$R in the tumor.

One limitation of our study should be pointed out. Overexpression of AT$_1$R may be present in other kinds of tumors, such as cervical cancer and adrenal pheochromocytoma. Thus, it is difficult to differentiate hepatocellular carcinoma from other kinds of tumors in the liver tissue.

In conclusion, our study indicated that ^{131}I-anti-AT$_1$R mAb enables non-invasive evaluation of hepatocellular carcinoma specifically and may be a new potential molecular imaging agent for targeting tumor.

Author Contributions

Conceived and designed the experiments: PPH YPL GHH. Performed the experiments: PPH YPL CYY TL CZ JS. Analyzed the data: PPH YPL JKH. Contributed reagents/materials/analysis tools: PPH YPL. Wrote the paper: PPH YPL.

References

1. Forner A, Llovet JM, Bruix J (2012) Hepatocellular carcinoma. Lancet 379: 1245–1255.
2. Ferlay J, Shin HR, Bray F, Forman D, Mathers C, et al. (2010) Estimates of worldwide burden of cancer in 2008: GLOBOCAN 2008. Int J Cancer 127: 2893–2917.
3. Singal A, Volk ML, Waljee A, Salgia R, Higgins P, et al. (2009) Meta-analysis: surveillance with ultrasound for early-stage hepatocellular carcinoma in patients with cirrhosis. Aliment Pharmacol Ther 30: 37–47.
4. Lok AS, Sterling RK, Everhart JE, Wright EC, Hoefs JC, et al. (2010) Des-gamma-carboxy prothrombin and alpha-fetoprotein as biomarkers for the early detection of hepatocellular carcinoma. Gastroenterology 138: 493–502.
5. Colli A, Fraquelli M, Casazza G, Massironi S, Colucci A, et al. (2006) Accuracy of ultrasonography, spiral CT, magnetic resonance, and alpha-fetoprotein in diagnosing hepatocellular carcinoma: a systematic review. Am J Gastroenterol 101: 513–523.
6. Liang T, Zhang C, Song J, Jiang S, Hao J, et al. (2011) Evaluation of ^{131}I-anti-MIF mAb as a reporter for allograft rejection. Clin Immunol 139: 40–47.
7. Dinh DT, Frauman AG, Sourial M, Casley DJ, Johnston CI, et al. (2001) Identification, distribution, and expression of angiotensin II receptors in the normal human prostate and benign prostatic hyperplasia. Endocrinology 14: 1349–1356.
8. Takeda H, Kondo S (2001) Differences between squamous cell carcinoma and keratoacanthoma in angiotensin type-1 receptor expression. Am J Pathol 158: 1633–1637.
9. Kikkawa F, Mizuno M, Shibata K, Kajiyama H, Morita T (2004) Activation of invasiveness of cervical carcinoma cells by angiotensin II. Am J Obstet Gynecol 190: 1258–1263.
10. Suganuma T, Ino K, Shibata K, Kajiyama H, Nagasaka T (2005) Functional expression of the angiotensin II type 1 receptor in human ovarian carcinoma cells and its blockade therapy resulting in suppression of tumor invasion, angiogenesis, and peritoneal dissemination, Clin Cancer Res. 11: 2686–2694.
11. Won SM, Park YH, Kim HJ, Park KM, Lee WJ (2006) Catechins inhibit angiotensin II-induced vascular smooth muscle cell proliferation via mitogen-activated protein kinase pathway. Exp Mol Med 38: 525–534.
12. Kosaka T, Miyajima A, Takayama E, Kikuchi E, Nakashima J, et al. (2007) Angiotensin II type 1 receptor antagonist as an angiogenic inhibitor in prostate cancer. Prostate 67: 41–49.
13. Zhang C, Hou G, Liang T, Song J, Qu L, et al. (2007) A prospective study of macrophage migration inhibitory factor as a marker of inflammatory detection. J Cell Mol Med 13: 4077–4083.
14. Zhao Q, Yan P, Wang RF, Zhang CL, Li L, et al. (2013) A novel $^{99\ m}$Tc-labeled molecular probe for tumor angiogenesis imaging in hepatoma xenografts model: a pilot study. PLoS One 8: e61043.
15. Bonde MM, Hansen JT, Sanni SJ, Haunsø S, Gammeltoft S, et al. (2010) Biased signaling of the angiotensin II type 1 receptor can be mediated through distinct mechanisms. PLoS One 5: e14135.
16. Wu C, Wei J, Tian D, Feng Y, Miller RH, et al. (2008) Molecular Probes for Imaging Myelinated White Matter in CNS. J Med Chem 51: 6682–6688.
17. Jonathan S Wall, Stephen J Kennel, Angela Williams, Tina Richey, Alan Stuckey, et al. (2012) AL Amyloid Imaging and Therapy with a Monoclonal Antibody to a Cryptic Epitope on Amyloid Fibrils. PLoS One 7: e52686.
18. Ozeki K, Tanida S, Morimoto C, Inoue Y, Mizoshita T, et al. (2013) Telmisartan inhibits cell proliferation by blocking nuclear translocation of ProHB-EGF C-terminal fragment in colon cancer cells. PLoS One 8: e56770.
19. Khakoo AY, Sidman RL, Pasqualini R, Arap W (2008) Does the renin-angiotensin system participate in regulation of human vasculogenesis and angiogenesis? Cancer Res 68: 9112–9115.
20. Farazi PA, DePinho RA (2006) Hepatocellular carcinoma pathogenesis: from genes to environment. Nat Rev Cancer 6: 674–687.
21. Villanueva A, Newell P, Chiang DY, Friedman SL, Llovet JM (2007) Genomics and signaling pathways in hepatocellular carcinoma. Semin Liver Dis 27: 55–76.
22. Heffelfinger SC (2007) The renin angiotensin system in the regulation of angiogenesis. Curr Pharm Des 13: 1215–1229.
23. Willis LM, El-Remessy AB, Somanath PR, Deremer DL, Fagan SC (2011) Angiotensin receptor blockers and angiogenesis: clinical and experimental evidence. Clin Sci 120: 307–319.
24. Tahmasebi M, Barker S, Puddefoot JR, Vinson GP (2006) Localisation of renin-angiotensin system (RAS) components in breast. Br J Cancer 95: 67–74.
25. Lau ST, Leung PS (2011) Role of the RAS in pancreatic cancer. Curr Cancer Drug Targets 11: 412–420.
26. Koh SL, Ager EI, Christophi C (2010) Liver regeneration and tumour stimulation: implications of the rennin-angiotensin system. Liver Int 30: 1414–1426.
27. Dzau VJ, Mukoyama M, Pratt RE (1994) Molecular biology of angiotensin receptors: target for drug research? J Hypertens Suppl 12: S1–S5.
28. Fujita M, Hayashi I, Yamashina S, Fukamizu A, Itoman M, et al. (2005) Angiotensin type 1a receptor signaling dependent induction of vascular endothelial growth factor in stroma is relevant to tumor-associated angiogenesis and tumor growth. Carcinogenesis 26: 271–279.